

Derivation and differentiation of haploid human embryonic stem cells

Ido Sagi¹, Gloryn Chia², Tamar Golan-Lev¹, Mordecai Peretz¹, Uri Weissbein¹, Lina Sui², Mark V. Sauer³, Ofra Yanuka¹, Dieter Egli^{2,4} & Nissim Benvenisty¹

Diploidy is a fundamental genetic feature in mammals, in which haploid cells normally arise only as post-meiotic germ cells that serve to ensure a diploid genome upon fertilization. Gamete manipulation has yielded haploid embryonic stem (ES) cells from several mammalian species^{1–6}, but haploid human ES cells have yet to be reported. Here we generated and analysed a collection of human parthenogenetic ES cell lines originating from haploid oocytes, leading to the successful isolation and maintenance of human ES cell lines with a normal haploid karyotype. Haploid human ES cells exhibited typical pluripotent stem cell characteristics, such as self-renewal capacity and a pluripotency-specific molecular signature. Moreover, we demonstrated the utility of these cells as a platform for loss-of-function genetic screening. Although haploid human ES cells resembled their diploid counterparts, they also displayed distinct properties including differential regulation of X chromosome inactivation and of genes involved in oxidative phosphorylation, alongside reduction in absolute gene expression levels and cell size. Surprisingly, we found that a haploid human genome is compatible not only with the undifferentiated pluripotent state, but also with differentiated somatic fates representing all three embryonic germ layers both *in vitro* and *in vivo*, despite a persistent dosage imbalance between the autosomes and X chromosome. We expect that haploid human ES cells will provide novel means for studying human functional genomics and development.

Haploid genetics is useful for delineating genome function. Although haploid genetics has been mostly restricted to unicellular organisms, recent reports of haploid ES cells have extended it into animal species, including mammals^{1–7}. Deriving haploid human ES cells by similar approaches has probably been hindered by the limited availability of human oocytes⁸. Artificial activation of unfertilized metaphase II (MII) human oocytes results in efficient development to the blastocyst stage and subsequent derivation of parthenogenetic ES (pES) cells^{9–11}. In mouse parthenogenetic embryos haploidy usually persists at the blastocyst stage^{12,13}, but diploid cells progressively dominate over increasing cell cycles due to spontaneous and irreversible diploidization^{13–15} (Fig. 1a). By estimation, even if diploidization occurs in 1 out of 10 cell cycles, 1% of ES cells may remain haploid at early passages (Extended Data Fig. 1a).

To explore the feasibility of deriving haploid human ES cells, we generated and analysed a collection of 14 early-passage human pES cell lines for the persistence of haploid cells. We initially used chromosome counting by metaphase spreading as a method for unambiguous and quantitative discovery of rare haploid nuclei. Among ten individual pES cell lines, a low proportion of haploid metaphases was found in one cell line, pES10 (1.3%, Extended Data Table 1). In four additional lines, we also used viable fluorescence-activated cell sorting (FACS) with Hoechst 33342 staining, aiming to isolate cells with a DNA content

corresponding to less than two chromosomal copies (2c), leading to the successful enrichment of haploid cells from a second cell line, pES12 (Extended Data Table 2).

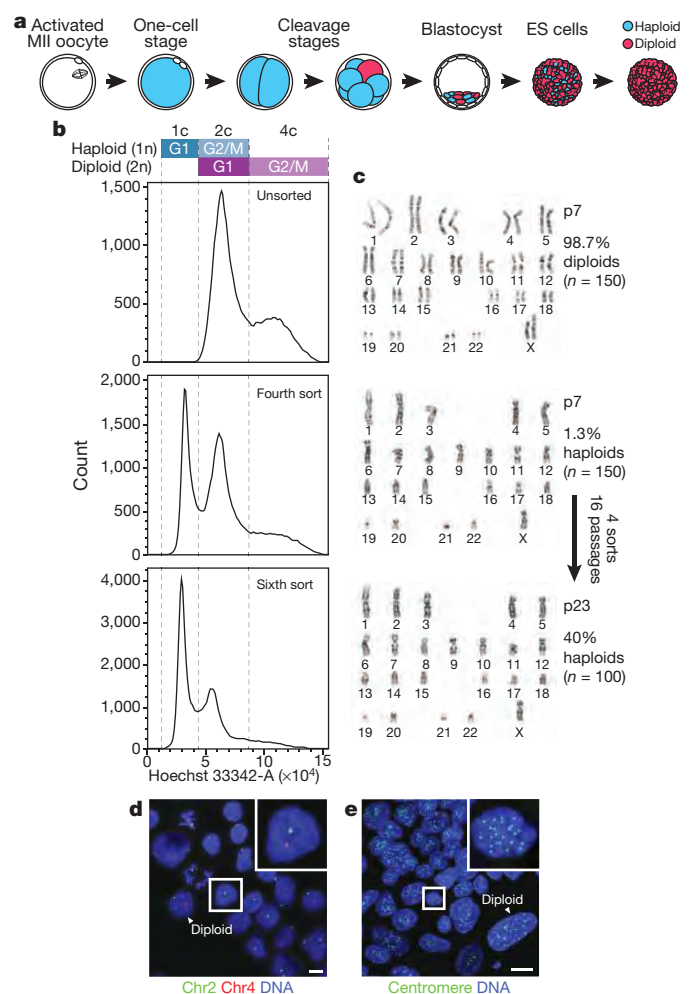


Figure 1 | Derivation of haploid human ES cells. **a**, Schematic of putative haploidy in pES cells. **b**, DNA content profiles of haploid pES10, established by repeated enrichment of 1c cells. Top to bottom, unsorted diploid cells, partially purified (fourth sort) and mostly purified (sixth sort) haploid cells. **c**, pES10 karyotypes before and after 1c-cell enrichment, *p*, passage. **d**, **e**, DNA FISH (**d**) and centromere staining (**e**) in haploid-enriched pES10 cells. Magnifications show haploid nuclei with a single hybridization signal (**d**) and 23 centromere foci (**e**), respectively. Scale bars, 10 μ m.

¹The Azrieli Center for Stem Cells and Genetic Research, Department of Genetics, Silberman Institute of Life Sciences, The Hebrew University, Jerusalem 91904, Israel. ²Department of Pediatrics, Columbia University, New York, New York 10032, USA. ³Center for Women's Reproductive Care, College of Physicians and Surgeons, Columbia University, New York, New York 10019, USA. ⁴The New York Stem Cell Foundation Research Institute, New York, New York 10032, USA.

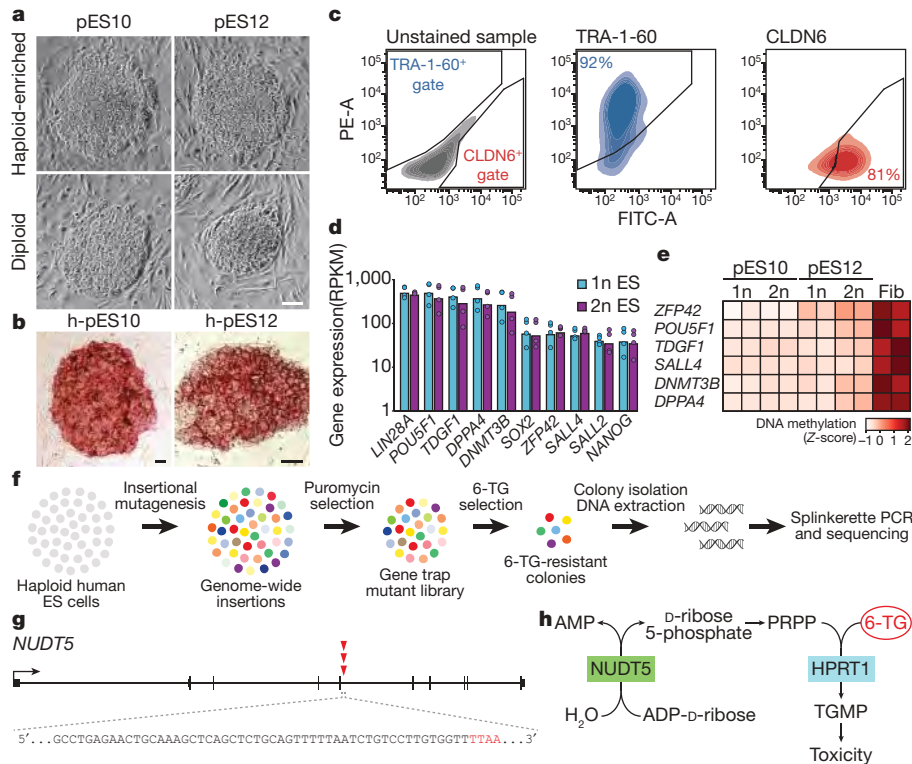


Figure 2 | Haploid human ES cells display pluripotent stem cell characteristics and enable loss-of-function screening. **a, b**, Colony morphology and alkaline phosphatase staining. Scale bars, 50 μ m. **c**, Flow cytometry analysis of gated h-pES10 1c cells by co-staining DNA and cell surface markers TRA-1-60 and CLDN6. **d**, Expression levels of pluripotency genes in G1-sorted haploid and diploid ES cells ($n = 4$ each,

two biological replicates per line, logarithmic scale). Mean indicated by bars. **e**, DNA methylation levels at pluripotency genes in biological duplicates of G1-sorted ES cells and control fibroblasts (Fib). **f**, Schematic of gene trapping and screening for 6-TG-resistance genes. **g**, *NUDT5* insertions (red arrows) detected in three 6-TG-resistant colonies (indicated by TTA). **h**, Metabolic pathway leading to 6-TG toxicity.

Two individual haploid-enriched ES cell lines were established from pES10 and pES12 (hereafter referred to as h-pES10 and h-pES12) within five to six rounds of 1c-cell enrichment and expansion (Fig. 1b and Extended Data Fig. 1b). These cell lines were cultured in standard conditions for over 30 passages while including cells with a normal haploid karyotype (Fig. 1c and Extended Data Fig. 1c). However, since diploidization occurred at a rate of 3–9% cells per day (Extended Data Fig. 1a; see Methods), sorting at every three to four passages was required to maintain haploid cells. Visualization of ploidy was further enabled by DNA fluorescence *in situ* hybridization (FISH) (Fig. 1d and Extended Data Fig. 1d) and quantification of centromere protein foci (Fig. 1e and Extended Data Fig. 1e; see Supplementary Notes and Extended Data Fig. 2). Besides having an intact karyotype, haploid ES cells did not harbour significant copy number variations (CNVs) relative to their unsorted diploid counterparts (Extended Data Fig. 1f), nor common duplications that would result in pseudo-diploidy, indicating that genome integrity was preserved throughout haploid-cell isolation and maintenance.

Both h-pES10 and h-pES12 exhibited classical human pluripotent stem cell features, including typical colony morphology and alkaline phosphatase activity (Fig. 2a, b). Single haploid ES cells expressed hallmark pluripotency markers as confirmed by centromere foci quantification in essentially pure (>95%) haploid cultures (Extended Data Fig. 3). Selective flow cytometry enabled the validation of the expression of two human ES-cell-specific cell surface markers (TRA-1-60 and CLDN6 (ref. 16)) in single haploid cells (Fig. 2c). Moreover, sorted haploid and diploid ES cells showed highly similar transcriptional and epigenetic signatures of pluripotency genes (Fig. 2d, e). In accordance with a parthenogenetic origin, these cells also featured distinct molecular profiles of maternal imprinting (Extended Data Fig. 4a–d).

Haploid cells are valuable for genetic screening because phenotypically selectable mutants can be identified upon disruption of single-copy alleles. To demonstrate the applicability of this principle in haploid human ES cells, we generated a genome-wide mutant library using a gene trap transposon system (Fig. 2f and Extended Data Fig. 4e; see Methods), and screened for resistance to the purine analogue 6-thioguanine (6-TG). Out of six isolated and analysed 6-TG-resistant colonies, three harboured an identical gene trap insertion at the *NUDT5* autosomal gene (Fig. 2g). The disruption of this gene was recently confirmed to confer 6-TG resistance in human cells¹⁷ (Fig. 2h). Detection of a loss-of-function phenotype due to an autosomal mutation thereby validates that genetic screening is feasible in haploid human ES cells.

The ability of human ES cells to exist as both haploids and diploids led us to investigate whether these two ploidy states differ in certain aspects of gene regulation and cell biology. To analyse haploid and diploid ES cells in the same cell cycle phase, we used FACS to isolate G1-phase haploid cells (1c) and compared them with isogenic G1-phase diploid cells (2c) from unsorted diploid cultures (Fig. 3a and Extended Data Fig. 5a; see Methods). We first aimed to uncover putative ploidy-associated differences by comparing the transcriptomes of haploid and diploid ES cells using RNA sequencing (RNA-seq), considering that observed changes in expression levels would be relative to the total gene expression of each ploidy state, rather than representing absolute differences. On the genome-scale, undifferentiated haploid and diploid ES cells clustered closely and separately from differentiated embryoid bodies (EBs) (Fig. 3b). Nonetheless, we identified 275 relatively upregulated and 290 relatively downregulated genes in haploids compared with diploids (greater than twofold change, false discovery rate (FDR) < 0.05; Extended Data Fig. 5b).

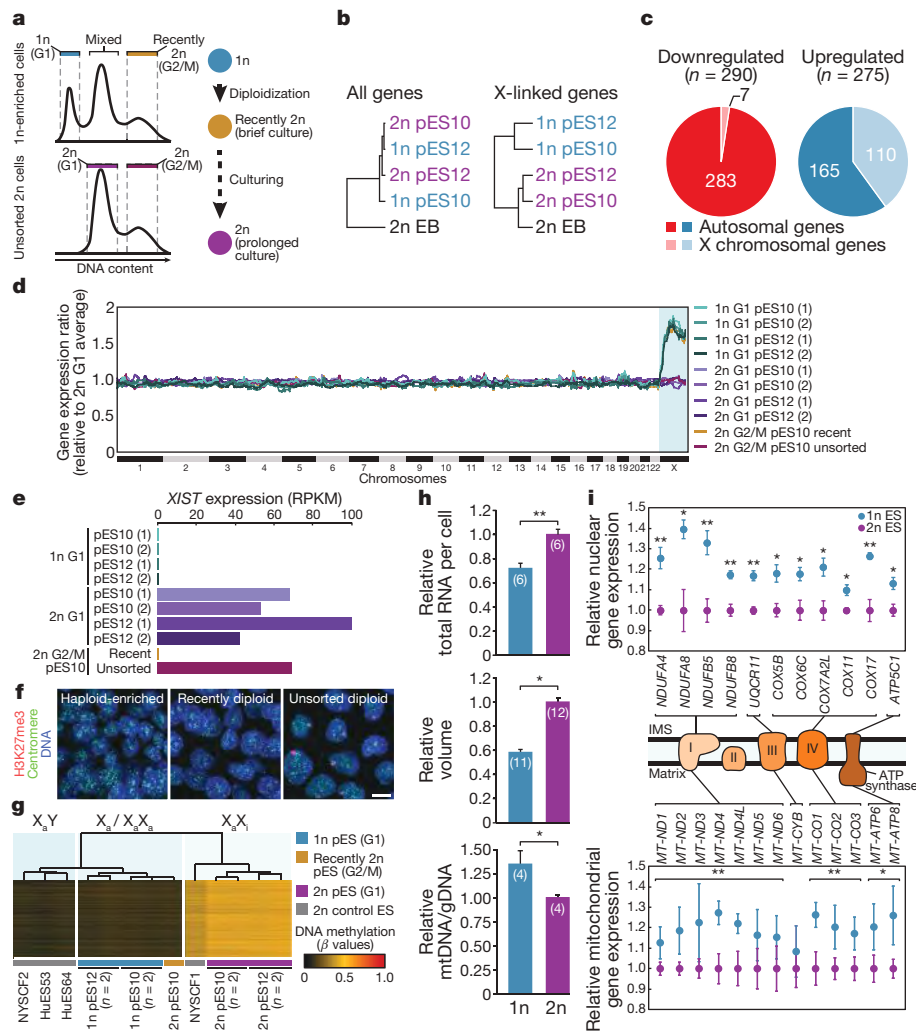


Figure 3 | Molecular and cellular comparisons of haploid and diploid ES cells. **a**, Experimental scheme. **b**, RNA-seq-based clustering analyses of isogenic G1-sorted haploid and diploid cells (two biological replicates per line) and diploid pES12-derived EBs. **c**, Pie chart of relatively downregulated and upregulated genes in haploid versus diploid ES cells. **d–g**, Differential X chromosome inactivation in haploid and diploid ES cells. **d**, Genome-wide expression moving median plot. **e**, *XIST* expression levels. **f**, H3K27me3 staining. Scale bar, 10 μ m. **g**, X chromosome DNA

Notably, X chromosomal genes were significantly overrepresented among the relatively upregulated gene set (40%, $P < 0.001$, χ^2 goodness of fit test) (Fig. 3c), and the expression levels of X chromosomal genes alone clearly distinguished between haploid and diploid ES cells (Fig. 3b). These data correlate with an expected differential status of X chromosome inactivation in haploid and diploid human ES cells: whereas the single-copy X chromosome in haploids is transcriptionally active (X_a), one of the two X chromosomes in diploids is often inactivated (X_aX_i)¹⁸. Indeed, haploid human ES cells exhibited a relative increase in X chromosomal gene expression and lacked expression of the *XIST* transcript which drives X chromosome inactivation (Fig. 3d, e and Extended Data Fig. 5b–d), as in diploid X_aX_a human ES cells¹⁹. X chromosome inactivation is regulated by repressive histone modifications and DNA methylation. H3K27me3 foci were consistently observed in unsorted diploid ES cells, but not in the haploid-enriched counterparts (Fig. 3f). Moreover, methylome analysis showed that the X chromosome DNA methylation signature of haploid ES cells resembles that of diploid male ES cells (X_aY), whose single-copy X chromosome is largely hypomethylated, as opposed to the composite pattern of a hypomethylated X_a and a hypermethylated X_i in diploid female cells

(Fig. 3g). Interestingly, recently diploidized ES cells (see Methods) remained X_aX_a soon after diploidization by all assays mentioned earlier (Fig. 3a, d–g). Normalization to total gene expression²⁰ resulted in seemingly similar expression levels of autosomal genes, but higher levels of X-linked genes in haploid cells (Fig. 3d and Extended Data Fig. 5c). However, assuming that the absolute expression of X-linked genes in haploid X_a and diploid X_aX_i cells are equivalent, these data suggest a genome-wide autosomal gene expression level reduction in haploids (Extended Data Fig. 5e, f). In support of this, total RNA amounts isolated from haploid ES cells were significantly lower than those from equal numbers of diploid cells (Fig. 3h). A decrease in total gene expression implied that physical dimensions may also be altered. Indeed, the average haploid:diploid diameter ratio of G1-sorted ES cells was ~ 0.8 , corresponding to ~ 0.7 surface area ratio and ~ 0.6 volume ratio (Fig. 3h and Extended Data Fig. 5g). We subsequently focused on consistent differential regulation within autosomes (see Methods). By transcriptome and methylome analyses, genes relatively downregulated in haploid ES cells were significantly enriched for genes encoding signal-peptide-bearing

methylation levels. **h**, Relative total RNA, cell volume and ratio of mitochondrial to genomic DNA (mtDNA/gDNA) between G1-sorted haploid and diploid ES cells. Number of replicates indicated in parenthesis. Error bars represent s.d. **i**, Mean expression levels \pm s.e.m. of nuclear and mitochondrial oxidative phosphorylation genes in haploid and diploid ES cells (replicates as in Fig. 2d), and their schematic organization in this pathway. * $P < 0.05$; ** $P < 0.01$ (two-tailed unpaired Student's *t* test). Source data for **h** and **i** are available online.

(Fig. 3g). Interestingly, recently diploidized ES cells (see Methods) remained X_aX_a soon after diploidization by all assays mentioned earlier (Fig. 3a, d–g). Normalization to total gene expression²⁰ resulted in seemingly similar expression levels of autosomal genes, but higher levels of X-linked genes in haploid cells (Fig. 3d and Extended Data Fig. 5c). However, assuming that the absolute expression of X-linked genes in haploid X_a and diploid X_aX_i cells are equivalent, these data suggest a genome-wide autosomal gene expression level reduction in haploids (Extended Data Fig. 5e, f). In support of this, total RNA amounts isolated from haploid ES cells were significantly lower than those from equal numbers of diploid cells (Fig. 3h). A decrease in total gene expression implied that physical dimensions may also be altered. Indeed, the average haploid:diploid diameter ratio of G1-sorted ES cells was ~ 0.8 , corresponding to ~ 0.7 surface area ratio and ~ 0.6 volume ratio (Fig. 3h and Extended Data Fig. 5g).

We subsequently focused on consistent differential regulation within autosomes (see Methods). By transcriptome and methylome analyses, genes relatively downregulated in haploid ES cells were significantly enriched for genes encoding signal-peptide-bearing

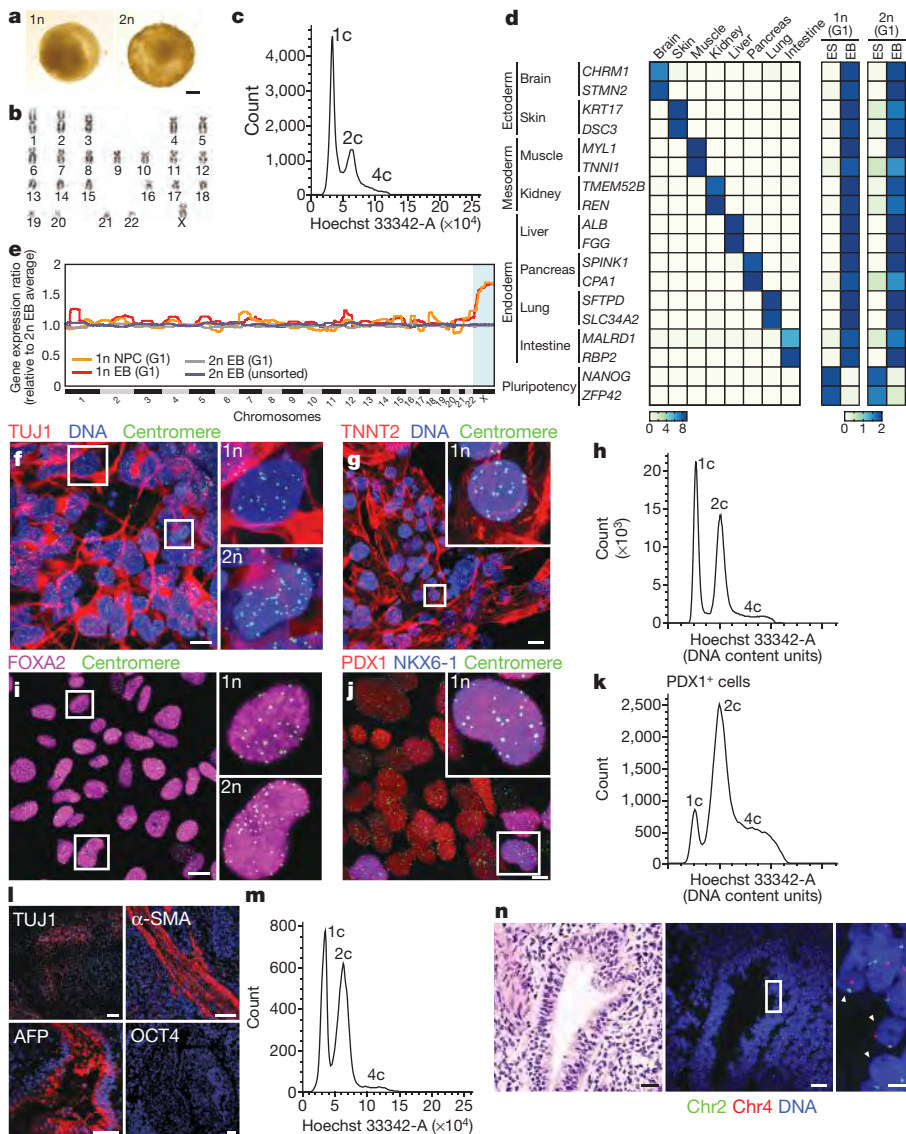


Figure 4 | Differentiation of haploid human cells. **a**, EBs from haploid-enriched and diploid pES12 cells. Scale bar, 100 μ m. **b**, Haploid EB cell karyotype. **c**, DNA content profile of h-pES10 EB cells. **d**, Expression of tissue- and pluripotency-specific genes in G1-sorted haploid and diploid ES and EB pES10 cells. **e**, Differential X chromosome inactivation in haploid and diploid EBs and NPCs by genome-wide expression moving median plot. **f**, **g**, **i**, **j**, Centromere and differentiation marker co-staining in h-pES12-derived neurons (**f**), cardiomyocytes (**g**), definitive endoderm cells (**i**) and pancreatic cells (**j**). Scale bars, 10 μ m. **h**, **k**, DNA content profiles of h-pES12 cells differentiated into cardiomyocytes (**h**) and PDX1-positive pancreatic cells (**k**). **l**, TUJ1 (ectoderm), α -SMA (mesoderm), AFP (endoderm) and OCT4 (pluripotency) staining in an h-pES12-derived teratoma. Scale bars, 50 μ m. **m**, DNA content profile of an h-pES10-derived teratoma. **n**, Serial h-pES12-derived teratoma sections analysed histologically (left; scale bar, 20 μ m) and by DNA FISH (middle; scale bar, 20 μ m). Haploid nuclei are shown in magnification (right; scale bar, 5 μ m).

proteins (Extended Data Fig. 5h). Remarkably, we also detected subtle yet significant relative upregulation of 11 genes involved in oxidative phosphorylation in haploid cells, including representatives encoding subunits of four out of the five complexes comprising this pathway (Fig. 3i and Extended Data Fig. 5i). Furthermore, all 13 mitochondrially encoded oxidative phosphorylation genes were consistently upregulated as well (Fig. 3i), indicating coordinated regulation between nuclear and mitochondrial genes. This coincided with a 32% increase in the mitochondrial DNA (mtDNA) to nuclear DNA ratio between haploids and diploids (Fig. 3h), suggesting that mitochondrial abundance relative to nuclear DNA content is higher in haploid cells.

We next sought to assess the differentiation potential of haploid human ES cells. The 21-day-old EBs generated by spontaneous differentiation of haploid-enriched and diploid ES cells could not be distinguished by their appearance (Fig. 4a), and the morphology of dissociated haploid-cell-derived EB cells was consistent with differentiation (Extended Data Fig. 6a). Notably, metaphase spreading revealed a haploid karyotype (Fig. 4b; 4/4 metaphases), and a largely haploid ($\sim 70\%$) DNA profile was confirmed by flow cytometry in both h-pES10-derived and h-pES12-derived EB cells (Fig. 4c and Extended Data Fig. 6b). We then compared the gene expression profiles of G1-sorted haploid ES cells and EB cells, focusing on 18 lineage-specific genes across nine cell types (Fig. 4d). Whereas expression levels were

negligible in undifferentiated ES cells, all tissue-specific genes were expressed in haploid and diploid EB cells (Fig. 4d and Extended Data Fig. 6c). Haploid and diploid EB cells showed insignificant expression of pluripotency-specific genes, consistent with efficient acquisition of differentiated cell fates.

To extend this analysis to more specific cell types, we subjected haploid ES cells to directed differentiation assays. Haploid ES cells differentiated towards a neural fate for ten days remained haploid, while giving rise to NCAM1-positive neural progenitor cells (NPCs, with $\sim 90\%$ efficiency) (Extended Data Fig. 7a, b). Sorted haploid NPCs expressed multiple neural-lineage-specific genes but not pluripotency-specific genes (Extended Data Fig. 7c, d). X chromosome inactivation in differentiated diploid female cells results in dosage compensation of 1:2 between the X chromosome and autosomes. As haploid cells do not inactivate their single-copy X chromosome, an X_a:autosomes dosage imbalance of 1:1 should persist into the differentiated state. Indeed, both haploid NPCs and EB cells showed an X_a signature contrary to the X_aX_i signature of diploid EB cells as indicated by whole-genome expression analysis and *XIST* levels (Fig. 4e and Extended Data Fig. 7e).

Neuronal differentiation was not restricted to the progenitor stage as the cells also differentiated with high efficiency ($>90\%$) into mature TUJ1 (also known as β -tubulin III)-positive neurons by 20 days, with persistence of haploid cells as shown by co-staining

with centromeres (Fig. 4f; 47% haploids, $n = 104$) and FISH analysis (Extended Data Fig. 7f, g; 46% haploids, $n = 200$). Similarly, haploid cells differentiated into TNNT2-expressing cardiomyocytes (Fig. 4g; 32% haploids, $n = 97$) during an eleven-day protocol resulting in spontaneously beating clusters (Supplementary Video 1), and 39% ($n = 31$) of haploid cells sorted from the whole culture (25% 1c-cells) were confirmed as TNNT2-positive (Fig. 4h and Extended Data Fig. 7h). Next, we differentiated haploid-enriched cultures (~70% haploids) to the pancreatic lineage. Analysing two stages of differentiation by centromere foci analysis, we observed robust differentiation (>90%) of both haploids and diploids into FOXA2-positive definitive endoderm cells (Fig. 4i; 56% haploids, $n = 112$), and differentiation into PDX1-positive pancreatic cells (Fig. 4j; 13% haploid, $n = 103$), some of which were also positive for NKX6-1. In addition, the persistence of haploid PDX1-positive cells was confirmed by flow cytometry (Fig. 4k; 10% PDX1-positive 1c cells; and Extended Data Fig. 7i, j).

Finally, both haploid-enriched human ES cell lines gave rise to teratomas comprising cell types of ectodermal, mesodermal and endodermal origins (Fig. 4l and Extended Data Fig. 8a, b), meeting the most stringent criterion for human pluripotency *in vivo*. Importantly, no residual undifferentiated OCT4-positive cells were detected (Fig. 4l and Extended Data Fig. 8b). Upon dissection, DNA content analysis revealed that a considerable population of h-pES10-derived teratoma cells remained haploid (Fig. 4m). Combined analysis of serial sections from an independent, h-pES12-derived teratoma, by histology and FISH confirmed the existence of *in vivo* differentiated haploid human cells capable of contributing to an organized tissue structure while responding to developmental signals (Fig. 4n). Haploid cells were identified in all analysed teratomas ($n = 4$), albeit with variable proportions, which may be influenced by the initial amount of haploid cells and/or the duration of teratoma formation.

Haploid mammalian cells have proven invaluable for loss-of-function screens⁷. Using a genome-wide library of gene-trapped haploid human ES cells, we demonstrated their potential for biomedically relevant functional genomics by forward genetic screening (Supplementary Discussion). Whereas previous studies on non-human haploid ES cells mostly emphasized the similarity between haploids and diploids, here we also pointed to several transcriptional, epigenetic and physical properties that set them apart (Supplementary Discussion). Interestingly, we did not observe global transcriptional compensation in haploid cells, indicating that it is not required for cellular viability as long as an autosomal balance is preserved. In contrast, autosomal imbalance appears intolerable based on the strict absence of human autosomal monosomies in *in vitro* fertilization ES cells²¹. Remarkably, we found that a haploid human karyotype is not a barrier for ES cell differentiation. As observed in the mouse², haploid human ES cells gave rise to NPCs while remaining haploid. However, while mouse studies showed that haploid cells are lost upon further differentiation^{2,14}, we observed specification of human haploid cells into somatic cell fates of all three embryonic germ layers, despite persistent dosage imbalance between the X chromosome and autosomes (Supplementary Discussion).

Throughout evolution, mammalian genomes have been solidified by diploidy-dependent adaptations such as parental imprinting, which restrict the development of haploid uniparental embryos. Nonetheless, haploid cells are capable of directing development in certain animal species²². The surprising differentiation potential of haploid human genomes suggests that diploidy-dependent adaptations, rather than haploidy, pose the predominant barriers for uniparental development in humans. The discovery of haploid human ES cells should thus provide novel means to delineate basic aspects of human genetics and development.

Online Content Methods, along with any additional Extended Data display items and Source Data, are available in the online version of the paper; references unique to these sections appear only in the online paper.

Received 30 July 2015; accepted 8 February 2016.

Published online 16 March 2016.

1. Leeb, M. & Wutz, A. Derivation of haploid embryonic stem cells from mouse embryos. *Nature* **479**, 131–134 (2011).
2. Elling, U. *et al.* Forward and reverse genetics through derivation of haploid mouse embryonic stem cells. *Cell Stem Cell* **9**, 563–574 (2011).
3. Yang, H. *et al.* Generation of genetically modified mice by oocyte injection of androgenetic haploid embryonic stem cells. *Cell* **149**, 605–617 (2012).
4. Li, W. *et al.* Androgenetic haploid embryonic stem cells produce live transgenic mice. *Nature* **490**, 407–411 (2012).
5. Li, W. *et al.* Genetic modification and screening in rat using haploid embryonic stem cells. *Cell Stem Cell* **14**, 404–414 (2014).
6. Yang, H. *et al.* Generation of haploid embryonic stem cells from *Macaca fascicularis* monkey parthenotes. *Cell Res.* **23**, 1187–1200 (2013).
7. Wutz, A. Haploid mouse embryonic stem cells: rapid genetic screening and germline transmission. *Annu. Rev. Cell Dev. Biol.* **30**, 705–722 (2014).
8. Egli, D. *et al.* Impracticality of egg donor recruitment in the absence of compensation. *Cell Stem Cell* **9**, 293–294 (2011).
9. Revazova, E. S. *et al.* Patient-specific stem cell lines derived from human parthenogenetic blastocysts. *Cloning Stem Cells* **9**, 432–449 (2007).
10. Kim, K. *et al.* Recombination signatures distinguish embryonic stem cells derived by parthenogenesis and somatic cell nuclear transfer. *Cell Stem Cell* **1**, 346–352 (2007).
11. Paull, D. *et al.* Nuclear genome transfer in human oocytes eliminates mitochondrial DNA variants. *Nature* **493**, 632–637 (2013).
12. Tarkowski, A. K., Witkowska, A. & Nowicka, J. Experimental parthenogenesis in the mouse. *Nature* **226**, 162–165 (1970).
13. Kaufman, M. H., Robertson, E. J., Handyside, A. H. & Evans, M. J. Establishment of pluripotential cell lines from haploid mouse embryos. *J. Embryol. Exp. Morphol.* **73**, 249–261 (1983).
14. Leeb, M. *et al.* Germline potential of parthenogenetic haploid mouse embryonic stem cells. *Development* **139**, 3301–3305 (2012).
15. Takahashi, S. *et al.* Induction of the G2/M transition stabilizes haploid embryonic stem cells. *Development* **141**, 3842–3847 (2014).
16. Ben-David, U., Nudel, N. & Benvenisty, N. Immunologic and chemical targeting of the tight-junction protein Claudin-6 eliminates tumorigenic human pluripotent stem cells. *Nat. Commun.* **4**, 1992 (2013).
17. Doench, J. G. *et al.* Optimized sgRNA design to maximize activity and minimize off-target effects of CRISPR-Cas9. *Nature Biotechnol.* **34**, 184–191 (2016).
18. Silva, S. S., Rowntree, R. K., Mekhoubad, S. & Lee, J. T. X-chromosome inactivation and epigenetic fluidity in human embryonic stem cells. *Proc. Natl. Acad. Sci. USA* **105**, 4820–4825 (2008).
19. Bruck, T., Yanuka, O. & Benvenisty, N. Human pluripotent stem cells with distinct X inactivation status show molecular and cellular differences controlled by the X-linked ELK-1 gene. *Cell Rep.* **4**, 262–270 (2013).
20. Lovén, J. *et al.* Revisiting global gene expression analysis. *Cell* **151**, 476–482 (2012).
21. Biancotti, J. C. *et al.* The *in vitro* survival of human monosomies and trisomies as embryonic stem cells. *Stem Cell Res.* **9**, 218–224 (2012).
22. Otto, S. P. & Jarne, P. Evolution. Haploids—hapless or happening? *Science* **292**, 2441–2443 (2001).

Supplementary Information is available in the online version of the paper.

Acknowledgements We thank all members of the Benvenisty and Egli laboratories for input and support. We thank Y. Avior and W. Breuer for their assistance with experimental procedures. I.S. is supported by the Adams Fellowships Program for Doctoral Students, G.C. is supported by the A*STAR International Fellowship, U.W. is a Clore Fellow, D.E. is a NYSCF-Robertson Investigator, and N.B. is the Herbert Cohn Chair in Cancer Research. This work was partially supported by The Rosetrees Trust and by The Azrieli Foundation (to N.B.), by the Russell Berrie Foundation Program in Cellular Therapies of Diabetes, by the New York State Stem Cell Science (NYSTEM) IIRP Award number C026184, and by the New York Stem Cell Foundation (to D.E.).

Author Contributions I.S., D.E. and N.B. designed the study and wrote the manuscript with input from all authors. I.S. isolated and characterized haploid human ES cell lines, performed differentiation experiments and analysed the data. G.C. developed and performed the centromere quantification analysis and carried out neuronal differentiation. T.G.-L. assisted in tissue culture and performed karyotype analyses and tissue sectioning. I.S., M.P., U.W. and O.Y. were involved in the genetic screening. M.P. and U.W. assisted with teratoma assays. L.S. assisted with pancreatic differentiation. M.V.S. was involved in all aspects of oocyte donation and research. D.E. derived human pES cell lines from haploid oocytes. D.E. and N.B. supervised the study.

Author Information All high-throughput data have been deposited at the Gene Expression Omnibus (GEO) under accession number GSE71458. Reprints and permissions information is available at www.nature.com/reprints. The authors declare no competing financial interests. Readers are welcome to comment on the online version of the paper. Correspondence and requests for materials should be addressed to D.E. (de2220@cumc.columbia.edu) or N.B. (nissimb@cc.huji.ac.il).